JBC RESEARCH ARTICLE

A pGpG-specific phosphodiesterase regulates cyclic di-GMP signaling in *Vibrio cholerae*

Received for publication, September 2, 2021, and in revised form, January 18, 2022 Published, Papers in Press, January 21, 2022,
https://doi.org/10.1016/j.jbc.2022.101626

Kyoo Heo[1,‡], Jae-Woo Lee[1,‡], Yongdae Jang[2], Sohee Kwon[3], Jaehun Lee[1], Chaok Seok[3], Nam-Chul Ha[2,*], and Yeong-Jae Seok[1,*]

From the [1]School of Biological Sciences and Institute of Microbiology, [2]Department of Agricultural Biotechnology, Research Institute for Agriculture and Life Sciences, Center for Food and Bioconvergence, and [3]Department of Chemistry, Seoul National University, Seoul, Republic of Korea

Edited by Chris Whitfield

The bacterial second messenger bis-(3′-5′)-cyclic diguanylate monophosphate (c-di-GMP) controls various cellular processes, including motility, toxin production, and biofilm formation. c-di-GMP is enzymatically synthesized by GGDEF domain–containing diguanylate cyclases and degraded by HD-GYP domain–containing phosphodiesterases (PDEs) to 2 GMP or by EAL domain–containing PDE-As to 5′-phosphoguanylyl-(3′,5′)-guanosine (pGpG). Since excess pGpG feedback inhibits PDE-A activity and thereby can lead to the uncontrolled accumulation of c-di-GMP, a PDE that degrades pGpG to 2 GMP (PDE-B) has been presumed to exist. To date, the only enzyme known to hydrolyze pGpG is oligoribonuclease Orn, which degrades all kinds of oligoribonucleotides. Here, we identified a pGpG-specific PDE, which we named PggH, using biochemical approaches in the gram-negative bacteria *Vibrio cholerae*. Biochemical experiments revealed that PggH exhibited specific PDE activity only toward pGpG, thus differing from the previously reported Orn. Furthermore, the high-resolution structure of PggH revealed the basis for its PDE activity and narrow substrate specificity. Finally, we propose that PggH could modulate the activities of PDE-As and the intracellular concentration of c-di-GMP, resulting in phenotypic changes including in biofilm formation.

Bis-(3′-5′)-cyclic diguanylate monophosphate (c-di-GMP) is a widely conserved bacterial second messenger found in all major bacterial phyla (1). It was first discovered in 1987 as an activator of the cellulose synthase from *Komagataeibacter xylinus* (formerly known as *Gluconacetobacter xylinus*) by Ross *et al.* (2). c-di-GMP is associated with diverse cellular processes, such as bacterial growth, motility, virulence, biofilm formation, and cell cycle progression (3). Low levels of cellular c-di-GMP upregulate motility by inducing flagellar expression, assembly, or motor function (4) and are also required for the expression of acute virulence genes (5). In contrast, high c-di-GMP levels stimulate the biosynthesis of fimbriae, adhesins, various matrix exopolysaccharides, and biofilm formation (4, 6, 7). Moreover, c-di-GMP–dependent spatiotemporal control of protein degradation is crucial in cell cycle progression in *Caulobacter crescentus* (8).

c-di-GMP is synthesized from two GTP molecules by diguanylate cyclases harboring the GGDEF domain, named after its conserved motif Gly-Gly-Asp-Glu-Phe (3). The degradation of c-di-GMP is mediated by two types of phosphodiesterases (PDEs) containing either the HD-GYP or EAL domain (9). HD-GYP domain proteins hydrolyze c-di-GMP to two molecules of GMP in a one-step reaction (10). In contrast, EAL domain-containing PDEs (PDE-As) degrade c-di-GMP into the linear product 5′-phosphoguanylyl-(3′,5′)-guanosine (pGpG) (11, 12), requiring a second PDE enzyme (PDE-B), which hydrolyzes pGpG into two GMP molecules, to complete the signaling process (13). In the two-step degradation mechanism *via* pGpG, the intermediate pGpG has been reported to competitively inhibit c-di-GMP-specific PDE-As catalyzing the first reaction by a feedback inhibition mechanism. The PDE activity of *Escherichia coli* YfgF, an EAL-containing PDE-A, has been found to be inhibited by high concentrations of pGpG (14). Furthermore, pGpG acts as a competitive inhibitor of the EAL-containing response regulator RocR and inhibits c-di-GMP turnover in *Pseudomonas aeruginosa* (15). These findings suggest that the appropriate degradation of pGpG by PDE-B is crucial for sustaining the c-di-GMP signaling pathway.

Recently, a high-throughput DRaCALA-based screen on a *Vibrio cholerae* El Tor N16961 complete genome ORF library has revealed several pGpG-binding proteins including oligoribonuclease VC0341 (hereafter *Vc*Orn), as well as EAL and HD-GYP domain proteins, and some proteins of unknown functions. Of these, *Vc*Orn, which possesses an RNase-T domain (Fig. 1*A*), was then determined to exhibit pGpG PDE activity, similar to the previous findings in *P. aeruginosa* (16–18). However, unlike its ortholog in *P. aeruginosa*, *Vc*Orn has been shown to be an essential exonuclease (19), similar to that in *E. coli*, which is responsible for the degradation of nanoRNAs, from di-ribonucleotides to penta-ribonucleotides (20). Thus, the pGpG-hydrolyzing function of this protein appeared to be a part of RNA turnover (18). In most bacteria, the intracellular concentration of c-di-GMP is acutely

‡ These authors contributed equally to this work.
*For correspondence: Yeong-Jae Seok, yjseok@snu.ac.kr; Nam-Chul Ha, hanc210@snu.ac.kr.

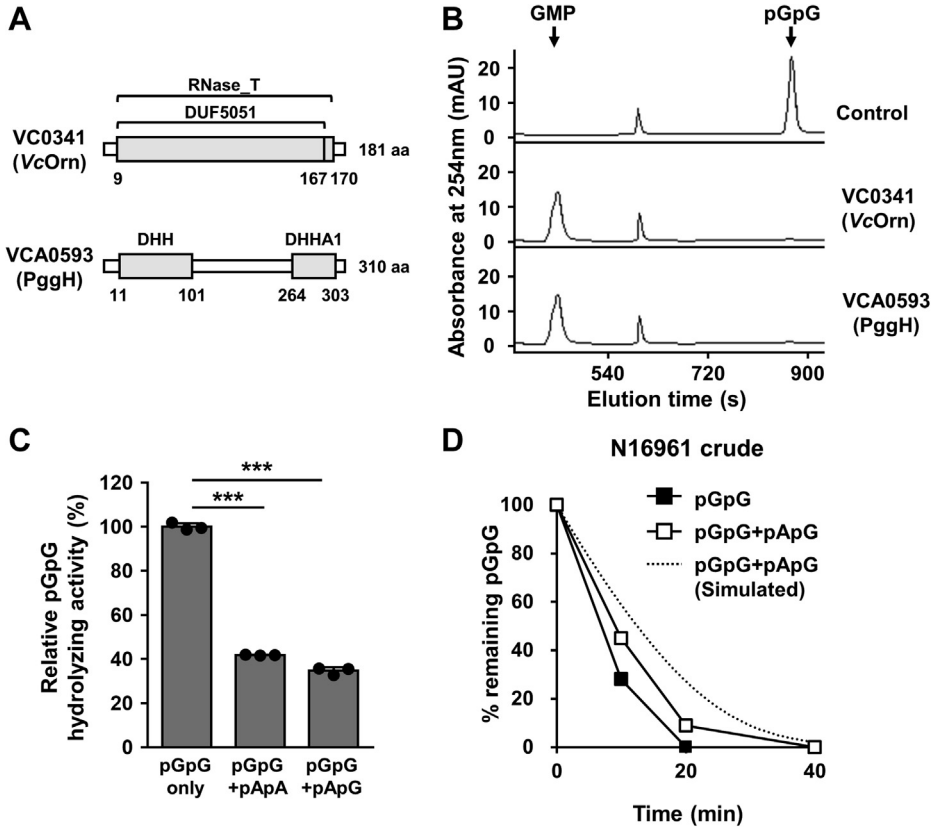

Figure 1. VCA0593 hydrolyzes pGpG to GMP. *A,* schematic depiction of the domain structures of VC0341 and VCA0593. VC0341 possesses an RNase_T domain found in a variety of exonuclease proteins, such as ribonuclease T and the epsilon subunit of DNA polymerase III. VCA0593 possesses DHH and DHHA1 domains present in DHH/DHHA1 family proteins, which have the conserved Asp-His-His motif in the active site at the N terminus and the sub-domain DHHA1 at the C terminus. *B,* degradation of pGpG (17.5 μM) to GMP by VC0341 and VCA0593 (2.2 μg each) was assessed by HPLC after incubation at 37 °C for 10 min. *C,* the pGpG hydrolase activity of *V. cholerae* Orn was evaluated in the presence of the indicated ribonucleotides (20 μM pGpG; 100 μM pApG and pApA). *D,* degradation of pGpG (20 μM) by cell lysates from WT *V. cholerae* N16961 was assessed in the absence (*open square*) and presence (*closed square*) of excess amounts of pApG (100 μM) at the indicated time points. The simulated inhibitory effect of pApG on the pGpG-hydrolyzing activity was calculated based on the Michaelis–Menten equation (*dotted line*). Statistical significance was assessed using Student's *t* test (***p value <0.005). Shown are means and SDs (n = 3, independent measurements). pGpG, 5′-phosphoguanylyl-(3′,5′)-guanosine.

modulated by the specific activities of its metabolic enzymes responding to the environmental signals (4). Therefore, we speculated whether *Vc*Orn could degrade pGpG rapidly enough to meet diverse metabolic needs and thus fulfill the role of a PDE-B which is responsible for the c-di-GMP signal decay in *V. cholerae,* even in the presence of nanoRNAs. These considerations prompted us to search for a PDE-B that is primarily responsible for the degradation of pGpG in the c-di-GMP signaling network.

Here, we report that *V. cholerae* VCA0593 is a pGpG-specific PDE-B that is highly conserved within the genus *Vibrio*. Through comparison between VCA0593 and other DHH/DHHA1 family enzymes, which are involved in the hydrolysis of oligonucleotides in various bacterial species, we discuss the structural basis for the narrow substrate specificity of VCA0593 and its role as a modulator of cellular c-di-GMP levels in *V. cholerae*.

Results

Oligoribonuclease activity of V. cholerae *Orn*

First, we determined the exonuclease activity of purified *Vc*Orn using several nanoRNAs, including pGpG as a substrate (Fig. 1*B*; Table 1). Similar to its ortholog in *E. coli*, *Vc*Orn could hydrolyze nanoRNAs including pentaribonucleotides 5′-GGAAA-3′ and 5′-AAAAA-3′, albeit at a considerably slower rate than the diribonucleotides, pApA, pApG, and pGpG, which is consistent with a previous study (18). We then tested whether the pGpG-hydrolyzing activity of *Vc*Orn would be affected by other nanoRNAs. We found that the pGpG-hydrolyzing activity of *Vc*Orn was inhibited in the

Table 1
Substrate specificity of PggH and Orn

Substrate	Specific activity (μmol/mg/min)	
	PggH	Orn
pAp	0	0
c-di-GMP	0	0
c-di-AMP	0	0
AAAAA	0	0.25 ± 0.03
GGAAA	0	0.26 ± 0.05
ssDNA	0	n.d.
pApA	0	0.34 ± 0.01
pApG	0	0.32 ± 0.02
pGpG	0.20 ± 0.01	0.35 ± 0.01

PggH, phosphoguanylyl guanylate hydrolase; n.d., not determined; Orn, oligoribonuclease.

presence of excess amounts of pApA, pApG, and 5′-GGAAA-3′ (Figs. 1*C* and S1). This inhibition by other nanoRNAs was also observed when we measured the pGpG-degrading activity of WT *V. cholerae* N16961 cell crude extract in the absence and presence of excess amounts of pApG (Fig. 1*D*). Interestingly, we found that the inhibitory effect of pApG on the pGpG-hydrolyzing activity of the crude extract was significantly lower than that simulated based on the result in Figure 1*C*. These results led us to speculate the existence of another pGpG-binding protein(s) responsible for the specific degradation of pGpG in *V. cholerae*.

pGpG-specific PDE activity of PggH

VCA0593 has also been reported to bind pGpG in *V. cholerae* El Tor N16961 (15). An analysis of the primary structure of VCA0593 revealed that this protein possesses DHH (residues 11–101) and DHHA1 (residues 264–303) domains (Fig. 1*A*). Therefore, it can be classified as a DHH/DHHA1 family enzyme. The DHH/DHHA1 family enzymes are involved in the hydrolysis of oligonucleotides in various bacterial species (21), such as the *Thermotoga maritima* PDE TM1595, which hydrolyzes various linear dinucleotides (22); PDE YybT, which hydrolyzes cyclic dinucleotides (c-di-GMP and c-di-AMP) (23); the 3′-phosphoadenosine 5′-phosphate (pAp) phosphatase YtqI (24) in *Bacillus subtilis*; and the ssDNA exonuclease RecJ, which is highly conserved in most bacterial and archaea (25). Thus, we assumed that VCA0593 might exhibit nucleotide-hydrolyzing activity. First, we assessed the PDE activity of VCA0593 toward several known substrates of DHH/DHHA1 family proteins; c-di-GMP, c-di-AMP, pAp, and ssDNA (Table 1). However, these substrates were not hydrolyzed by VCA0593. We then examined the oligoribonuclease activity of VCA0593 toward the pentaribonucleotides 5′-GGAAA-3′ and 5′-AAAAA-3′ and the diribonucleotides pApA, pApG, and pGpG. Although VCA0593 exhibited PDE activity toward pGpG, neither the pentaribonucleotides nor the diribonucleotides pApA and pApG were degraded by VCA0593 (Fig. 1*B*; Table 1), suggesting that, unlike *Vc*Orn and TM1595 that hydrolyze other linear dinucleotides as well as pGpG, VCA0593 is a PDE that specifically hydrolyzes pGpG. Therefore, we named it PggH (**p**hospho**g**uanylyl **g**uanylate **h**ydrolase). PggH is highly conserved only among species of the genus *Vibrio* (Fig. S2). A protein BLAST search against the nonredundant protein sequences database at NCBI showed that the amino acid sequence identity of PggH was >77% among species of the genus *Vibrio* (26).

Most DHH/DHHA1 domain proteins function as homodimers, except the monomeric DNase RecJ (27). Gel filtration analysis revealed that PggH forms a homodimer (Fig. 2, *A* and *B*). PggH showed the highest PDE-B activity in the presence of Mn^{2+} among the divalent cations tested in this study (Fig. 2*C*). Thus, further biochemical studies were performed in the presence of Mn^{2+}. The Michaelis-Menten constant (K_m) and turnover number (k_{cat}) of PggH for pGpG were determined by analyzing the initial rate of pGpG hydrolysis at different substrate concentrations. A double-reciprocal plot of the pGpG-hydrolyzing activity of PggH showed K_m and k_{cat} values of 12.11 μM and 0.14 s^{-1}, respectively (Fig. 2, *D* and *E*). Since it has been previously shown that increasing the concentrations of pGpG over a range of 2 to 20 μM causes a progressive inhibition of c-di-GMP degradation by PDEs (13), the kinetic properties of PggH suggest that this enzyme might play a significant role in the c-di-GMP signal decay *in vivo*. Unlike that in *Vc*Orn, the pGpG-degrading activity of PggH was not substantially affected by nanoRNAs (Figs. 2*F* and S1), but interestingly, it showed a slight decrease in the presence of an excess amount of pApG.

Structural basis for pGpG PDE activity of PggH

To investigate the structural basis for the pGpG-specific PDE activity of PggH, we determined the crystal structure of the protein in the presence of Mn^{2+} at 1.9 Å resolution (Fig. 3). The asymmetric unit contained two protein molecules that closely interact with each other, consistently with the dimeric size in a gel filtration chromatography column (Fig. 2*B*). The two DHHA1 domains in the dimer formed a tight interaction, whereas no direct interaction between the DHH domains was found in the dimer (Fig. 3*A*). Each subunit contains a putative active site between the DHH and DHHA1 domains. The subunit structure further showed that Mn^{2+} is coordinated by Asp15, Asn55, His68, His69, and Asp121 at the active site, where His68 and His69 are from the conserved DHH motif (Fig. 3*B*). In addition, Asp13 and Asp67 are indirectly involved in the binding of Mn^{2+}, in a hydrogen bond network with Asn55 and His69, respectively. All these residues are strictly conserved among PggH homologs in *Vibrio* species (Fig. S2). Mutations at His68 and Asp121 completely abolished enzymatic activity, indicating that the coordination with divalent cation is essential for its activity as other DHH/DHHA1 family PDEs (Fig. S3) (21). Mutations at the two aspartate residues, Asp13 and Asp67, also abolished the enzymatic activity, implicating their importance in stabilizing the positions of the Mn^{2+}-coordinating residues (Fig. S3).

The DHHA1 domain of PggH contains a highly conserved GGGH motif, which is known to be responsible for the binding of nucleic acid in several enzymes of the DHH/DHHA1 family (22, 28). To examine the role of the GGGH motif in PggH, we mutated His282 to alanine. The mutation abolished pGpG hydrolysis activity of PggH, confirming the role of the GGGH motif in binding the nucleotide (Fig. S3).

By conducting structural comparisons with other DHH/DHHA1 domain–containing proteins, we found several unique features of PggH. While all other structure-annotated DHH/DHHA1 proteins including TM1595 form side-by-side butterfly-like dimers without any interference with an induced-fit model by the other subunit (22, 27–29), PggH forms a tightly intertwined dimer, apparently providing increased structural rigidity between the two subunits. The DHH and DHHA1 domains in one subunit are intervened by

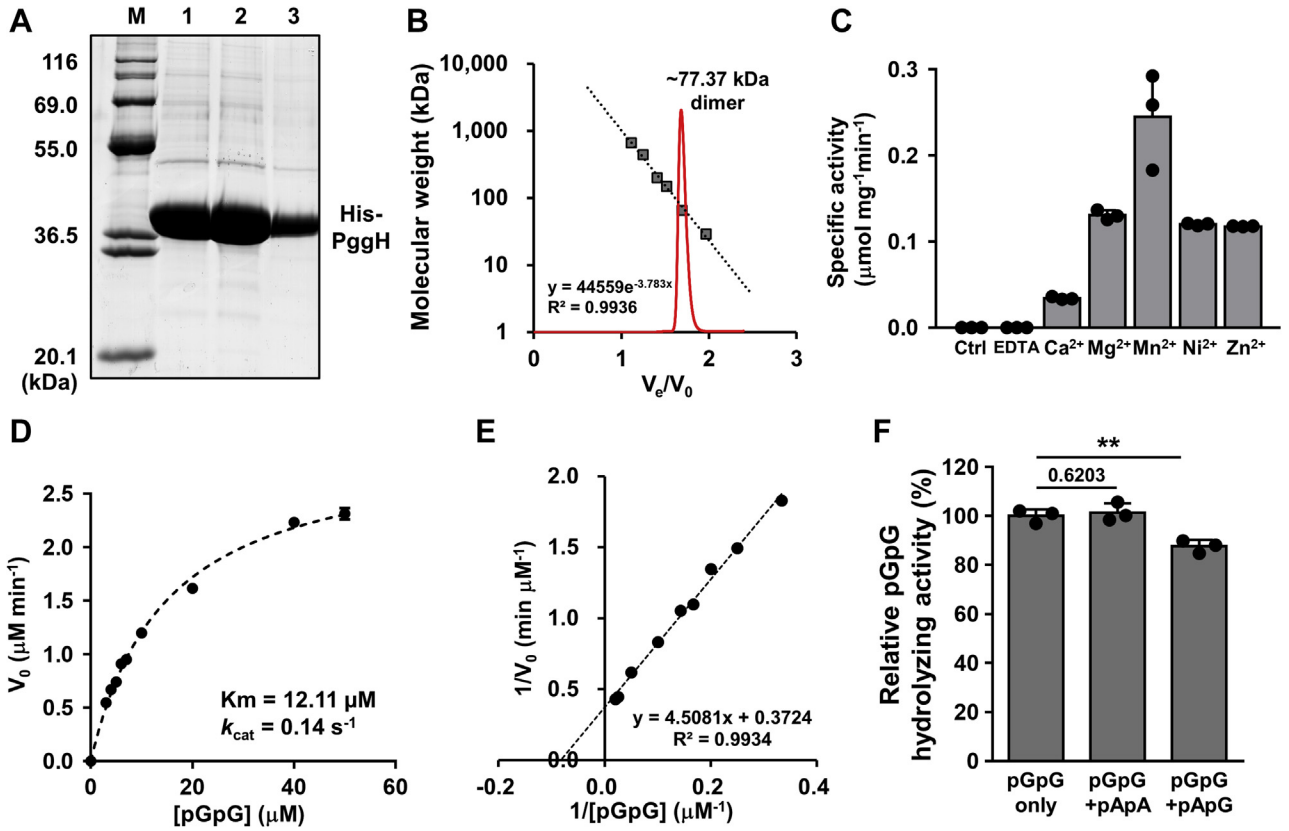

Figure 2. Purification and characterization of pGpG-hydrolyzing activity of PggH. *A,* His-tagged PggH was expressed and purified from *E. coli* and analyzed by SDS-PAGE followed by staining with Coomassie brilliant blue R. Lane M, molecular weight markers (KOMA Biotech); lanes 1 to 3, PggH-containing fractions eluted from a TALON metal affinity column. *B,* analysis of the oligomeric state of PggH by gel filtration chromatography using a HiLoad Superdex 200 column (26/600, GE Healthcare) in 25 mM Hepes–NaOH (pH 7.6) containing 100 mM NaCl, 5 mM β-mercaptoethanol. Molecular weight (MW) of PggH was estimated by extrapolating its elution volume to a linear plot of MW in a logarithmic scale *versus* elution volume of MW markers (thyroglobulin, 669 kDa; ferritin, 440 kDa; aldolase, 158 kDa; conalbumin, 75 kDa; ovalbumin, 44 kDa; carbonic anhydrase, 29 kDa; RNase A, 13.7 kDa; aprotinin, 6.5 kDa). PggH (*red line*) was eluted as a dimer of ∼77.37 kDa. *C,* effect of divalent cations on the pGpG phosphodiesterase activity of PggH (1.06 μg) was assessed by HPLC after 18 min incubation at 37 °C. Specific activity is expressed as the micromoles of GMP produced per minute per milligram of PggH. *D* and *E,* Michaelis–Menten and Lineweaver–Burk plots to determine the K_m and V_{max} of PggH. The initial velocity of pGpG hydrolysis (μM of GMP produced/min) was plotted as a function of the pGpG concentration. *F,* the pGpG hydrolase activity of *V. cholerae* PggH was evaluated in the presence of the indicated ribonucleotides (100 μM). Data shown in (*C*) and (*F*) are means and SDs (n = 3, independent measurements). Statistical significance was assessed using Student's *t* test (*p* value > 0.05 was presented, ***p* value < 0.01). pGpG, 5′-phosphoguanylyl-(3′,5′)-guanosine; PggH, phosphoguanylyl guanylate hydrolase.

the DHHA1 domain of the other subunit in the dimer (Fig. 3*C*). This domain arrangement reduces the space between the two subunits, which also appears to limit the mobility of the domains in response to the substrate binding. Structural rigidity was further found within the subunit. The DHH and DHHA1 domains in PggH are connected *via* a long rigid α-helix, which is also different from the canonical DHH/DHHA1 family phosphoesterases in which a flexible loop connects the two domains (Fig. 3*D*) (22, 28).

The molecular structures of TM1595 were determined both in the ligand-free form and in complex with the substrate pApA (22). A closing movement between DHH and DHHA1, which was induced by pApA binding was observed, demonstrating a typical example of the induced-fit model (30). However, compared to the flexible domain arrangement of other DHH/DHHA1 family proteins, the tightly intertwined domain arrangement of PggH would allow a very limited conformational change upon the binding of a substrate. (Fig. S4) Thus, our findings suggest that PggH could possess distinct mechanisms of substrate binding and its catalysis, which could explain the molecular basis underlying the narrow substrate specificity.

Mechanism of substrate selectivity of PggH

We then measured the binding affinity of PggH for linear diribonucleotides (pGpG, pApG, and pApA) using isothermal titration calorimetry (ITC) (Fig. S5) to further explore the mechanism of substrate specificity in more detail. Thermodynamic parameters indicated the enthalpy-driven interaction of PggH with pGpG (K_D = 14.13 ± 7.35 nM) and pApG (K_D = 104.67 ± 20.13 nM), whereas pApA did not bind to PggH (Figs. 4*A* and S5). These data suggested that the 3′-guanine in the substrate is crucial for the binding to PggH, whereas the 5′-guanine is essential for the formation of the active enzyme–substrate complex for catalysis. However, tetraribonucleotides with guanine at either 5′- or 3′-end did not bind PggH (Fig. S5), supporting that PggH has a narrow substrate specificity. Unfortunately, we were not able to test binding of trinucleotides to PggH, since we could not find any supplier.

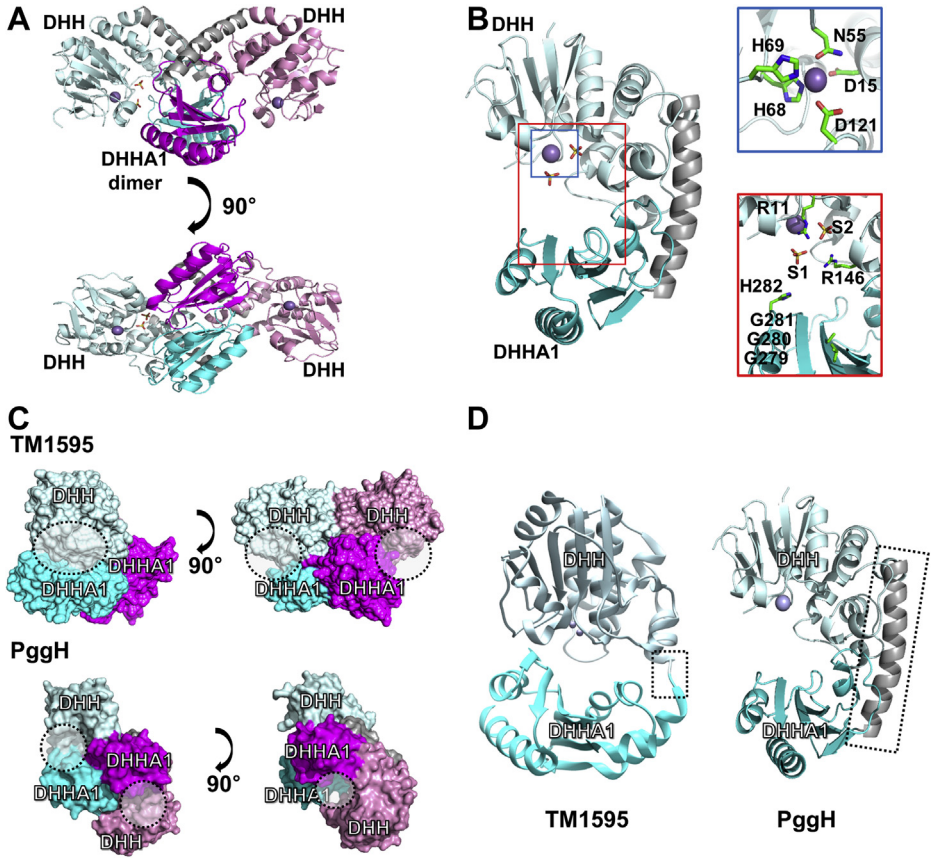

Figure 3. Crystal structure of PggH. *A,* overall structure of a PggH homodimer. Ribbon representations of the dimer structure of PggH. The two molecules are presented in different colors as follows: subunit *A* (DHH domain, *light cyan*; DHHA1 domain, *cyan*; α11 helix, *gray*) and subunit *B* (DHH domain, *pink*; DHHA1 domain, *magenta*; α11 helix, *gray*). *B,* the active site and the metal binding site. The active site is presented in a *red rectangle* and the metal binding site is presented in a *blue rectangle* (*left*). Detailed views of the active site and metal binding site are presented *right*. Metal coordinating residues are colored *green*, two sulfates are colored *yellow*, and a Mn^{2+} ion is presented as a *purple sphere* in (*A*) and (*B*). *C,* comparison of the dimeric structures between TM1595 and PggH. Surface representations of the homodimeric structures of TM1595 and PggH. The DHH domains are colored *light cyan* and *pink*. The DHHA1 domains are colored *cyan* and *magenta*. The active sites between the DHH and DHHA1 domains are presented as *dotted black circles*. *D,* ribbon representations of the monomeric structures of TM1595 and PggH. The DHH domains are colored *light cyan* and the DHHA1 domains are colored *cyan*. The linker helix of PggH is colored *gray*. Metal ions are represented as *purple spheres*. The linker loop of TM1595 and the linker helix of PggH are highlighted as *dotted black rectangles*. PggH, phosphoguanylyl guanylate hydrolase.

To identify the crucial residues required for substrate binding, we generated five PggH variants in which the hydrophilic residues in the putative active site were mutated and measured binding affinities of these mutants for pGpG and pApG, respectively (Fig. 4*A*). Interestingly, mutation of His282 to alanine led to a significantly decreased binding affinity (by > 10-fold) for pGpG, but it showed a similar affinity for pApG, compared to that shown by the WT protein. These data explain the reason why the PggH(H282A) mutant completely lost pGpG hydrolase activity (Fig. S3), suggesting that His282 is critical for the recognition of 5′-guanine for the catalysis. In contrast, the substitution of Arg11 with alanine decreased the binding affinity for pApG without affecting that for pGpG, implying that Arg11 is critical for binding to the noncognate substrate pApG. These differential mutational effects on the cognate and noncognate substrates suggest that pGpG has a different binding configuration to pApG by tethering of 5′-guanine to His282, which determines the catalytic activity of PggH. Moreover, we found two arginine residues involved in the binding of the dinucleotides. The R146A mutant showed a significantly lower binding affinity for both pGpG and pApG, while the Arg228 mutant exhibited no binding to the two dinucleotides, indicating that these two arginine residues might be involved in the recognition of 3′-guanine. Although Asp121 coordinates Mn^{2+} and thus is essential for the catalytic activity, mutation in this residue did not significantly affect the binding affinity for pGpG and pApG, implying that Asp121 is not involved in the substrate binding.

Based on these mutation analyses, we simulated the binding models of the PggH crystal structure to pGpG and pApG using Galaxydock3 software, a protein-ligand docking program (Fig. 4, *B* and *C*) (31). In these models, 3′-guanosine of both pGpG and pApG are bound in a narrow cleft surrounded by Arg228, Arg146, and Asn227. The guanidinium group of Arg228 forms hydrogen bonds with N3 and the amide group of Asn146 with N7 of 3′-guanine. Meanwhile, according to the docking models, the side chain carbonyl oxygen of Asn227 forms hydrogen bonds with the N1 imino proton and the C2 amine group of 3′-guanine. Because N1 is not protonated and there is no amino group at C2 in adenine, dinucleotides with

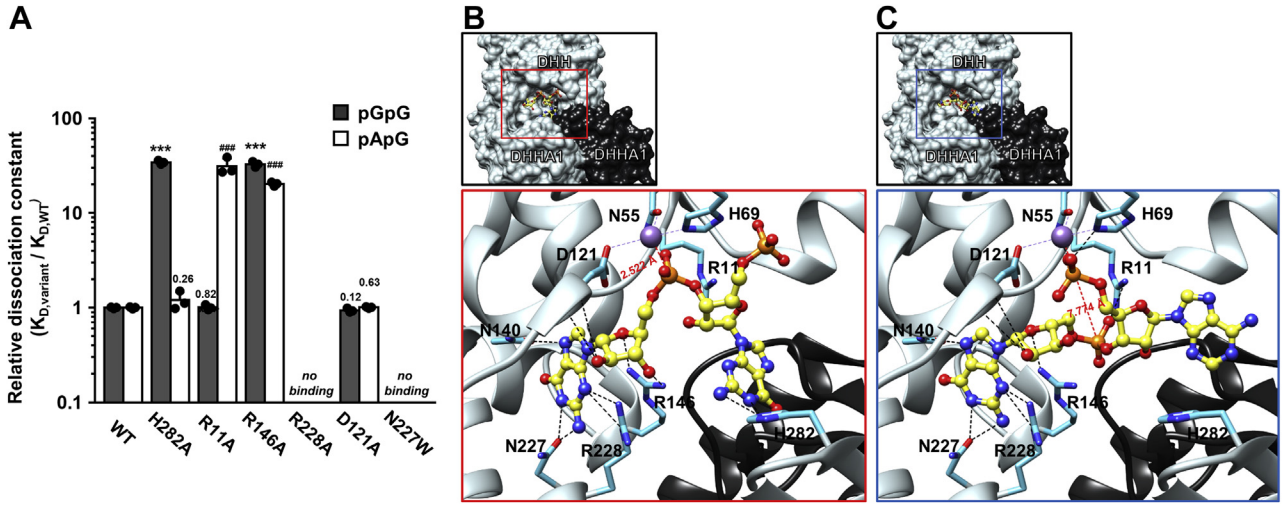

Figure 4. PggH distinguish its substrate at two stages. *A,* binding affinities of PggH and its variants for the pGpG and pApG were measured using isothermal titration calorimetry (ITC). Titration experiments consisted of a single initial injection of 1 μl, followed by 13 injections of 2 μl nucleotides (100 μM pGpG and pApG) in 25 mM Hepes–NaOH (pH 7.6), 100 mM NaCl, and 1 mM EDTA into the reaction cell containing 10 μM His-PggH or the same amount of its variant (H282A, R11A, R146A, R228A, D121A, and N227W) in the same buffer. The dissociation constants were obtained using MicroCal PEAQ-ITC Analysis Software with a single-site binding model. Data shown are means and SDs (n = 3, independent measurements). Statistical significance was assessed using Student's *t* test *versus* WT (*p* values > 0.05 were presented, ***p values < 0.005 for pGpG group; $^{\#\#\#}p$ values < 0.005 for pApG group). *B* and *C,* the binding pose of pGpG (*B*) and pApG (*C*) in the binding pocket of PggH was simulated using Galaxydock3 software. Overall simulated models are presented in small rectangles (*top*). Active sites of PggH are presented in *red* and *blue rectangles* in pGpG- and pApG-bound forms, respectively, and detailed views of the active sites are presented below. The *black dotted lines* indicated the hydrogen bonds between nucleotides and amino acid residues. The distance between the phosphorus atom of the phosphodiester bond (*orange*) and Mn^{2+} ion (*purple*) is indicated by the *red dotted line* along with the value. pGpG, 5′-phosphoguanylyl-(3′,5′)-guanosine; PggH, phosphoguanylyl guanylate hydrolase.

3′-adenine, such as pApA, may not be recognized by Asn227, at least partly accounting for the substrate selectivity of PggH at the 3′-base of the diribonucleotide. When we substituted Asn227 with tryptophan, we were unable to detect any binding of pGpG and pApG to PggH, supporting the simulated docking model. The substrate binding is further stabilized by several hydrogen bonds between ribose of 3′-guanosine with the guanidinium group of Arg146 and backbone carboxyl groups of Gly120 and Asp121. This was supported by the ITC data, which showed that the mutation at Arg146 reduced the binding affinity for both pGpG and pApG.

Recognition of the base at the 5′-position appears to be accomplished by His282 of the GGGH motif. The formation of hydrogen bonds between Nε2 of His282 and the N1 and C2 amine groups of 5′-guanine introduced a bend in the pGpG molecule, rendering the phosphodiester bond more accessible to Mn^{2+} ion (∼2.6 Å). However, because 5′-adenine could not form hydrogen bonds with His282, pApG remained in a straight configuration. In this pose, the distance between phosphate and Mn^{2+} was not adequately close to allow a nucleophilic attack by a Mn^{2+}-activated water molecule (∼7.8 Å). This structural model indicated that binding with His282 is indispensable for the appropriate positioning of the substrate (Fig. 4*B*).

PggH is involved in the regulation of c-di-GMP signaling

Because our results indicated that PggH is a pGpG-specific PDE with its intrinsic structural nature, we compared pGpG hydrolysis activities between the cell lysates from WT and a *pggH*-deficient mutant (Δ*pggH*) strains to evaluate the pGpG degradation by cellular PggH (Fig. 5*A*). Lysates of the *pggH* mutant still degraded pGpG into GMP, suggesting that there exist additional proteins possessing pGpG-hydrolase activity, including *Vc*Orn and some RNases (32). However, the deletion of *pggH* significantly decreased the pGpG-hydrolyzing activity of cell lysates, indicating that PggH plays a substantial role in hydrolyzing pGpG in *V. cholerae* cells.

Previous biochemical studies revealed that the accumulation of pGpG could inhibit the c-di-GMP PDE activity of PDE-As (13) and suggested that appropriate degradation of pGpG is required for the maintenance of the c-di-GMP signaling. Thus, we speculated whether PggH could regulate the c-di-GMP signaling in *V. cholerae*. To assess the effect of PggH on the regulation of the c-di-GMP concentration, we compared intracellular concentrations of pGpG and c-di-GMP between the WT and a *pggH*-deficient mutant (Fig. 5*B*). Quantification using LC-MS/MS revealed that Δ*pggH* cells had an approximately 2.6-fold higher concentration of pGpG than WT cells, indicating that PggH possesses the pGpG PDE activity in *V. cholerae* cells. We also found a higher level of c-di-GMP in Δ*pggH* cells compared to that in WT cells, leading to the conclusion that PggH is involved in regulating the c-di-GMP signaling.

To examine the role of PggH in this signaling pathway, we measured biofilm formation, which requires a high level of c-di-GMP (33, 34). We observed that Δ*pggH* cells exhibited a higher biofilm-forming activity than WT cells, indicating that PggH negatively regulates the c-di-GMP signaling in the cells (Fig. 5*C*). The *pggH*-complemented strain, constructed by transforming the PggH expression plasmid to the *V. cholerae pggH* mutant, exhibited a similar level of biofilm formation

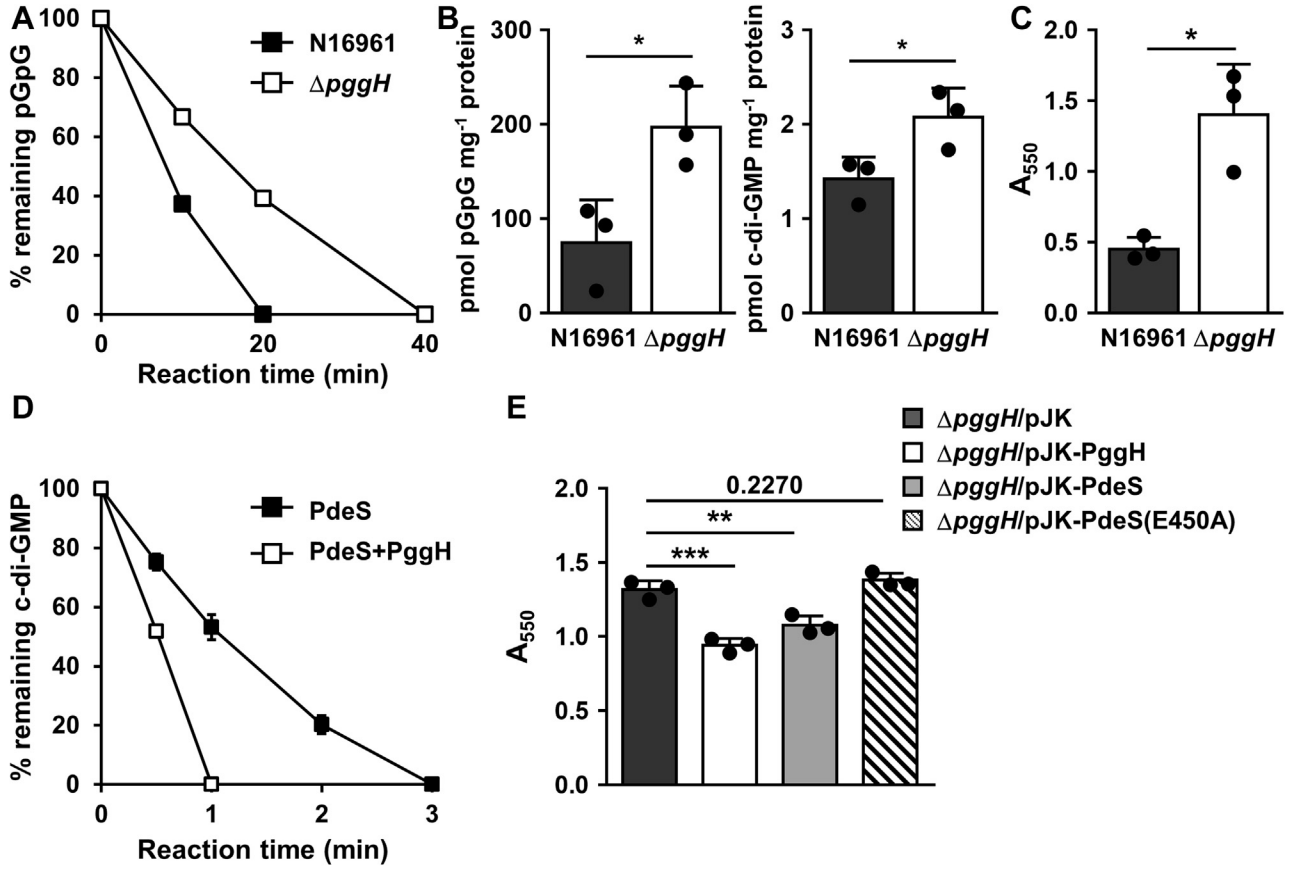

Figure 5. PggH regulates c-di-GMP signaling. *A,* degradation of pGpG (20 μM) by cell lysates from WT *V. cholerae* N16961 and its otherwise isogenic Δ*pggH* strain was assessed at the indicated time points. *B,* the intracellular pGpG and c-di-GMP concentrations in WT *V. cholerae* N16961 and the Δ*pggH* mutant grown in LB medium were measured using LC-MS/MS(35). The measured concentrations were normalized to the total protein content. *C,* the biofilm-forming activity of WT N16961 and the Δ*pggH* strain was measured in LB medium. Biofilm was stained using a crystal violet staining method followed by determining at 550 nm. *D,* the c-di-GMP phosphodiesterase activity of PdeS was assessed in the absence and presence of PggH. The reaction mixtures of c-di-GMP (20 μM) and PdeS (4.8 μg) incubated in the absence and presence of PggH (5 μg) for 0.5, 1, 2, and 3 min were applied to a Supelcosil LC-18-HPLC column, followed by quantification of the remaining c-di-GMP as described under "Experimental procedures." *E,* indicated strains were incubated under static conditions in LB medium supplemented with 0.02% arabinose to induce the expression of PggH, PdeS, and PdeS(E450A), and the biofilm-forming activity was measured using a crystal violet staining method followed by determining at 550 nm. Statistical significance was assessed using Student's *t* test (*p* value >0.05 was presented, **p* value <0.05, ***p* value <0.01, ****p* value <0.005). Shown are means and SDs (n = 3, independent measurements). pGpG, 5′-phosphoguanylyl-(3′,5′)-guanosine; PggH, phosphoguanylyl guanylate hydrolase.

with that of the WT strain, whereas the *pggH* mutant strain expressing the biochemically inactive PggH(D13N) did not complement this phenotypic change. These results confirmed the regulatory role of PggH in c-di-GMP signaling through its pGpG-PDE activity (Fig. S6*A*). However, this modulatory effect was less significant in the *pggH* mutant carrying the *Vc*Orn expression plasmid (Fig. S6*B*). Therefore, it could be assumed that PggH can hydrolyze pGpG more efficiently than *Vc*Orn to relieve the feedback inhibition of c-di-GMP degradation.

PggH regulates c-di-GMP signaling in cooperation with PDE-As

It has been shown that c-di-GMP turnover by PDE-As is inhibited by pGpG (14, 15). To verify that the increased biofilm formation of the *pggH* mutant is associated with the inhibition of PDE-As by the accumulation of pGpG and thus the increased concentration of c-di-GMP, the c-di-GMP PDE activity of PDE-A was determined in the absence or presence of PggH *in vitro*. Recently, we identified a novel sugar-responsive PDE-A, named PdeS in *V. cholerae* (35). As the expression of PdeS increased in the stationary phase, that of PggH also increased (Fig. S7), and accordingly, we assumed that PdeS was suitable to assess the effects of PggH on the activity of PDE-As and the c-di-GMP signaling. As expected, the PDE activity of PdeS was stimulated by the addition of PggH (Fig. 5*D*), suggesting that the product pGpG inhibits the activity of PDE-A by a negative feedback mechanism and that PggH functions as a modulator of PDE-A by controlling the pGpG level. We then constructed a *pggH* mutant expressing the c-di-GMP PDE PdeS and measured biofilm formation, using pJK1113 plasmid which possesses an arabinose-inducible P_{BAD} promoter of *araBAD* operon upstream of a multiple cloning site (Fig. 5*E*). Compared to the *pggH* mutant carrying pJK1113, cells carrying pJK-PdeS exhibited an apparent decrease in biofilm formation to a level similar to that of cells carrying pJK-PggH. However, the *pggH* mutant harboring pJK-PdeS(E450A), which expresses an inactive form of PdeS (35), did not exhibit the rescued phenotype, indicating that the *pggH* mutant accumulates c-di-GMP. The decreased biofilm

formation of the *pggH* mutant was also observed when we transformed the mutant with an expression vector for VieA, a well-studied PDE (Fig. S6*B*) (12). Based on these findings, we concluded that PggH regulates c-di-GMP signaling by modulating the overall activities of PDE-As in *V. cholerae*.

Discussion

The degradation of oligoribonucleotides by nanoRNases is a critical process for cell physiology in terms of RNA recycling and the completion of cyclic nucleotide signaling. In Gammaproteobacteria, the only protein previously identified to degrade diribonucleotides is the oligoribonuclease Orn, and its regulatory roles in c-di-GMP signaling have been well studied in *P. aeruginosa* (15, 18). However, in bacterial species in which Orn is essential for cell growth, such as *E. coli* and *V. cholerae*, whether Orn is involved in cyclic nucleotide signaling has not been clearly determined.

In this study, we investigated two proteins that have been reported to bind pGpG in the *V. cholerae* ORFeome from the DRaCALA-based screen (15). Biochemical analysis suggests that Orn and PggH cooperate to reduce the cellular pGpG level and ensure the timely decay of the c-di-GMP signal, as a high level of pGpG inhibits the c-di-GMP PDE activity of PDE-As in *V. cholerae* (13–15). PggH exhibits a lower K_m value than Orn (PggH, 12.11 μM; Orn, 41.15 μM), in addition to a considerably lower K_{cat} value (PggH, 0.14 s^{-1}; Orn, 23.33 s^{-1}) (Figs. 2, *D* and *E* and S8). Considering that Orn has a variety of substrates from diribonucleotides to pentaribonucleotides present at similar levels in the cell, whereas pGpG specifically digests pGpG and its activity is little affected in the presence of other nanoRNAs, it can be assumed that optimal pGpG hydrolysis activity of the two proteins would be exerted in the cell under different physiological contexts. At higher pGpG concentrations, Orn might play the major role in the hydrolysis of pGpG as well as other nanoRNAs, whereas PggH likely plays a role in the degradation of pGpG under physiological pGpG concentrations to allow for a finer tuning of the c-di-GMP signaling network. This notion is consistent with our result that the ectopic expression of either PggH or Orn in the Δ*pggH* mutant reduced biofilm formation by ∼29% and ∼13%, respectively (Fig. S6*B*). These data suggest that PggH could play a pivotal role in the degradation of pGpG and the completion of c-di-GMP signaling in their specific conditions in *V. cholerae*.

We determined the crystal structure of PggH at high resolution to gain molecular insights into the pGpG-specific activity of PggH. Most DHH/DHHA1 family PDEs show broad substrate specificity to various oligonucleotides, which could be explained by an induced-fit model accompanied by a large conformational change upon substrate binding (22, 28, 29). Compared to the open active site of these enzymes in the absence of substrate (apo state), PggH has a small and narrow active site. When we calculated the volume of active site of PggH and TM1595 using CASTp software with a probe radius of 2.5 Å, we found that PggH has an ∼2-fold smaller active site (383.796 $Å^3$) than TM1595 (748.513 $Å^3$). In addition, a rigid linker between the DHH and DHHA1 domains and the unique intervening dimeric arrangement of PggH further restrict the interdomain motion (Fig. 3). These distinct structural features lead to an unusually narrow substrate specificity of PggH compared to that shown by other DHH/DHHA1 family enzymes (Table 1, Figs. 2*F* and S1).

Linear dinucleotide intermediates can exhibit a regulatory effect on cyclic dinucleotide signaling. Here, we found that the degradation of pGpG by PggH is slightly inhibited in the presence of excess amounts of pApG (Fig. 2*F*) that can be produced following the degradation of 3′, 3′-cGAMP (36). Several enzymes have been reported to exhibit bifunctional activity that produces or degrades both c-di-GMP and cGAMP (37–39), suggesting that the concentration of two cyclic dinucleotides are interactively regulated. In this context, it is probable that PggH could act as a mediator in the cross talk between the c-di-GMP and cGAMP signaling pathway. Moreover, to the best of our knowledge, PggH is the first identified enzyme that specifically degrades pGpG. We therefore expect that further studies on the regulation of the pGpG hydrolysis activity of PggH might help to better understand the overall c-di-GMP signaling network in *V. cholerae*.

Experimental procedures

Bacterial strains, plasmids, and culture conditions

The bacterial strains, plasmids, and oligonucleotides used in this study are listed in Table S1 and S2. Bacterial cells were grown at 37 °C in LB medium. All plasmids were constructed using the standard polymerase chain reaction (PCR)-based cloning procedures and verified by sequencing.

To construct a *pggH* deletion mutant of the *V. cholerae* N16961 strain, the upstream and downstream regions of the *pggH* gene were amplified by PCR using the primer pairs PB421/PB422 and PB423/PB424, respectively. After digestion of the two PCR products, the XmaI-SphI and SphI-XbaI fragments, respectively, were cloned into the corresponding sites of the suicide vector pDM4 to generate the plasmid pDM4-PggH. The *E. coli* SM10 λ*pir* strain carrying pDM4-PggH was conjugated with *V. cholerae* N16961, and the transconjugants were selected. Integration was confirmed by PCR, and the exoconjugants were selected in LB containing 10% sucrose. Deletion of *pggH* in the selected colonies was confirmed by PCR (40, 41).

To construct pJK-P_{pggH}::*lacZ*, pJK1113 and the *pggH* promoter region was amplified by PCR using the primer pairs PB425/PB426 and PB427/PB428, respectively. And then, these PCR products were combined using the EZ-Fusion Cloning kit (Enzynomics). Then, the *lacZ* ORF amplified by PCR from *E. coli* chromosome using the primers PB429 and PB430 was digested with NcoI and SalI and inserted into the corresponding sites of pJK1113 (42, 43).

To construct pJK1113-VieA, pJK1113 and the *vieA* (VC1652) ORF region was amplified by PCR using the primer pairs PB437/PB438 and PB439/PB440, respectively. And then, these PCR products were combined using the EZ-Fusion Cloning kit.

Purification of proteins

His-tagged proteins (His-PggH and His-Orn) were expressed in the *E. coli* ER2566 strain by adding 1 mM IPTG and incubating at 30 °C for 4 h. The proteins were purified using TALON metal affinity resin according to the manufacturer's instructions (Takara Bio). After elution with buffer A (20 mM Hepes–NaOH (pH 7.6), 100 mM NaCl, 5 mM β-mercaptoethanol, and 5% glycerol) containing 150 mM imidazole, His-tagged proteins were concentrated using Amicon Ultracel-3K centrifugal filters (Merck Millipore). To increase the purity of proteins (>98% pure) and remove imidazole, the concentrated fractions were subjected to gel filtration chromatography using a HiLoad 16/600 Superdex 200 column (GE Healthcare) equilibrated with buffer A (44, 45).

In vitro *assay for pGpG-hydrolyzing activity*

pGpG-hydrolyzing activity was assayed in a 100 μl reaction volume containing 50 mM Tris–HCl (pH 8.0), 10 mM $MnCl_2$, 250 mM NaCl, 5 mM β-mercaptoethanol, and indicated concentrations of pGpG and purified proteins. After incubation at 37 °C for the indicated time, the reaction was terminated by the addition of 20 mM EDTA, and then trifluoroacetic acid was added to a final concentration of 10%. The reaction product generated from pGpG was then analyzed by high-performance liquid chromatography (HPLC) using a Varian dual pump system connected to an ultraviolet–visible detector. A 20-μl reaction mixture was applied to a Supelcosil LC-18-T reverse phase chromatography column (Sigma Aldrich) equilibrated with 100 mM KH_2PO_4 and 8 mM tetrabutyl ammonium hydrogen sulfate (pH 2.6) in water and then chromatographed using a linear gradient of 0 to 30% methanol containing 100 mM KH_2PO_4 and 8 mM tetrabutyl ammonium hydrogen sulfate (pH 2.6) at a flow rate of 1 ml/min for 20 min. The eluted nucleotides were detected at 254 nm (46). The nuclease activities of PggH (1.51 μM) and Orn (2.55 μM) in Table 1 was assessed by incubating with the indicated nucleotides (15 μM), and the substrate and product were monitored for 15 min.

Assay for pGpG-hydrolyzing activity in cell lysates

V. cholerae cells grown in 10 ml LB medium were harvested at an A_{600} of ∼0.7 by centrifugation at 9000*g* at 4 °C for 10 min. The supernatant was discarded, and the pellet was resuspended in 600 μl PDE assay buffer, which contained 50 mM Tris–HCl (pH 8.0), 10 mM $MgCl_2$, 250 mM NaCl, 5 mM β-mercaptoethanol, and 1 mM PMSF. Then, cells were disrupted by two passages through a French pressure cell at 10,000 psi. pGpG was added to the lysate to a final concentration of 20 μM, and the mixture was divided into 100-μl aliquots. After aliquots were incubated at 37 °C for the indicated time, the reaction was terminated by the addition of 20 mM EDTA, and then trifluoroacetic acid was added to a final concentration of 10%. The reaction product generated from pGpG was then analyzed by HPLC (15).

Crystallization of PggH for structural determination

The crystals of the native protein were obtained as described previously (47). Briefly, the crystals were obtained by mixing the protein solution (1 μl, 10 mg/ml) and the reservoir solution (1 μl) containing 0.2 M magnesium chloride, Tris–HCl (pH 8.0), 12% PEG 4000, and 2 mM tris(2-carboxyethyl)phosphine hydrochloride at 14 °C by the vapor diffusion hanging-drop methods.

Structural determination and refinement

The crystals were transferred to cryoprotection buffer (2 μl, the reservoir solution supplemented with 30% glycerol) for 1 min and then were flash-cooled in liquid nitrogen for data collection under cryogenic conditions. To solve the phasing problem, 10 mM zinc chloride was added in cryoprotection buffer of several crystals. The datasets of Zn-soaked crystals were collected on a direct X-ray detector Pilatus 6M (Dectris), equipped in beamline 5C of Pohang Accelerator Laboratory, Republic of Korea, at a wavelength of 1.2822 Å and Mn^{2+} bound crystals at 0.9795 Å. The crystal of PggH belonged to the space group $P2_12_12$, with unit cell dimensions of a =68.4 Å, b = 148.3 Å, and c = 58.8 Å. The program HKL-2000 was employed to process, merge, and scale the diffraction datasets (48). Data collection statistics are provided in Table S3. Anomalous signals from four Zn sites were found in each subunit, and the resulting electron density map was sufficiently clear to build an initial model using the programs PHENIX and COOT (49, 50). The Mn^{2+}-bound structure was determined by direct refinement using the Zn^{2+}-soaked structure.

Isothermal titration calorimetry

All the ITC experiments were carried out at 25 °C using MicroCal PEAQ-ITC calorimeter (Malvern Panalytical). Each titration experiments consisted of a single initial injection of 1 μl, followed by 33 injections of 2 μl nucleotides (100 μM pGpG, pApG, and pApA) in 25 mM Hepes–NaOH (pH 7.6), 100 mM NaCl, and 1 mM EDTA into the reaction cell contained 10 μM His-PggH in the same buffer. The experimental data were analyzed using MicroCal PEAQ-ITC Analysis Software with a single-site binding model.

Measurement of biofilm formation

Overnight-cultured cells were 1:100 inoculated in buffered LB medium with potassium phosphate (pH 7.0) and incubated under static conditions in a 96-well polystyrene microtiter plate at 37 °C for 24 h. Planktonic cells were removed and washed away with PBS, and the biofilm-associated cells were stained using 0.1% crystal violet solution. After several rinses using PBS, the stained biofilm was eluted with 100% ethanol and measured at 550 nm (35).

Computational simulation of substrate binding

A protein–ligand docking program GalaxyDock3 (31) was used to predict the binding poses of pGpG and pApG to the PggH structure. To account for protein conformational

changes induced by substrate binding, alternative structures for the loops surrounding the binding site were generated using a loop modeling program GalaxyLoop (51). Multiple ensemble docking simulations of pGpG and pApG were performed on the protein structures generated by loop modeling, and the docking poses compatible with mutagenesis analyses were selected.

Data availability

Coordinates and structure factors have been deposited in the Protein Data Bank (PDB) under accession codes 7D62.

Supporting information—This article contains supporting information (35, 52–54).

Acknowledgments—This work was supported by the National Research Foundation Grants NRF-2018R1A5A1025077 and NRF-2019R1A2C2004143 funded by the Ministry of Science and ICT and by the Brain Korea 21 program.

Author contributions—K. H. and J.-W. L. conceptualization; K. H. and J.-W. L methodology; K. H., J.-W. L., Y. J., S. K., and J. L. investigation; K. H. writing-original draft, K. H., C. S., N.-C. H., and Y.-J. S. writing-review and editing; N.-C. H. and Y.-J. S. supervision. Y.-J. S. funding acquisition.

Conflict of interest—The authors declare that they have no conflicts of interest with the contents of this article.

Abbreviations—The abbreviations used are: c-di-GMP, bis-(3′-5′)-cyclic diguanylate monophosphate; ITC, isothermal titration calorimetry; PDE, phosphodiesterase; pGpG, 5′-phosphoguanylyl-(3′,5′)-guanosine; PggH, phosphoguanylyl guanylate hydrolase.

References

1. Romling, U., Galperin, M. Y., and Gomelsky, M. (2013) Cyclic di-GMP: The first 25 years of a universal bacterial second messenger. *Microbiol. Mol. Biol. Rev.* **77**, 1–52
2. Ross, P., Weinhouse, H., Aloni, Y., Michaeli, D., Weinberger-Ohana, P., Mayer, R., Braun, S., de Vroom, E., van der Marel, G. A., van Boom, J. H., and Benziman, M. (1987) Regulation of cellulose synthesis in *Acetobacter xylinum* by cyclic diguanylic acid. *Nature* **325**, 279–281
3. Jenal, U., Reinders, A., and Lori, C. (2017) Cyclic di-GMP: Second messenger extraordinaire. *Nat. Rev. Microbiol.* **15**, 271–284
4. Hengge, R. (2009) Principles of c-di-GMP signalling in bacteria. *Nat. Rev. Microbiol.* **7**, 263–273
5. Tamayo, R., Pratt, J. T., and Camilli, A. (2007) Roles of cyclic diguanylate in the regulation of bacterial pathogenesis. *Annu. Rev. Microbiol.* **61**, 131–148
6. Jenal, U., and Malone, J. (2006) Mechanisms of cyclic-di-GMP signaling in bacteria. *Annu. Rev. Genet.* **40**, 385–407
7. Romling, U., and Amikam, D. (2006) Cyclic di-GMP as a second messenger. *Curr. Opin. Microbiol.* **9**, 218–228
8. Duerig, A., Abel, S., Folcher, M., Nicollier, M., Schwede, T., Amiot, N., Giese, B., and Jenal, U. (2009) Second messenger-mediated spatiotemporal control of protein degradation regulates bacterial cell cycle progression. *Genes Dev.* **23**, 93–104
9. Schirmer, T., and Jenal, U. (2009) Structural and mechanistic determinants of c-di-GMP signalling. *Nat. Rev. Microbiol.* **7**, 724–735
10. Bellini, D., Caly, D. L., McCarthy, Y., Bumann, M., An, S. Q., Dow, J. M., Ryan, R. P., and Walsh, M. A. (2014) Crystal structure of an HD-GYP domain cyclic-di-GMP phosphodiesterase reveals an enzyme with a novel trinuclear catalytic iron centre. *Mol. Microbiol.* **91**, 26–38
11. Schmidt, A. J., Ryjenkov, D. A., and Gomelsky, M. (2005) The ubiquitous protein domain EAL is a cyclic diguanylate-specific phosphodiesterase: Enzymatically active and inactive EAL domains. *J. Bacteriol.* **187**, 4774–4781
12. Tamayo, R., Tischler, A. D., and Camilli, A. (2005) The EAL domain protein VieA is a cyclic diguanylate phosphodiesterase. *J. Biol. Chem.* **280**, 33324–33330
13. Cohen, D., Mechold, U., Nevenzal, H., Yarmiyhu, Y., Randall, T. E., Bay, D. C., Rich, J. D., Parsek, M. R., Kaever, V., Harrison, J. J., and Banin, E. (2015) Oligoribonuclease is a central feature of cyclic diguanylate signaling in *Pseudomonas aeruginosa*. *Proc. Natl. Acad. Sci. U. S. A.* **112**, 11359–11364
14. Lacey, M. M., Partridge, J. D., and Green, J. (2010) *Escherichia coli* K-12 YfgF is an anaerobic cyclic di-GMP phosphodiesterase with roles in cell surface remodelling and the oxidative stress response. *Microbiology (Reading)* **156**, 2873–2886
15. Orr, M. W., Donaldson, G. P., Severin, G. B., Wang, J., Sintim, H. O., Waters, C. M., and Lee, V. T. (2015) Oligoribonuclease is the primary degradative enzyme for pGpG in *Pseudomonas aeruginosa* that is required for cyclic-di-GMP turnover. *Proc. Natl. Acad. Sci. U. S. A.* **112**, E5048–E5057
16. Niyogi, S. K., and Datta, A. K. (1975) A novel oligoribonuclease of *Escherichia coli*. I. Isolation and properties. *J. Biol. Chem.* **250**, 7307–7312
17. Zhang, X., Zhu, L., and Deutscher, M. P. (1998) Oligoribonuclease is encoded by a highly conserved gene in the 3′-5′ exonuclease superfamily. *J. Bacteriol.* **180**, 2779–2781
18. Kim, S. K., Lormand, J. D., Weiss, C. A., Eger, K. A., Turdiev, H., Turdiev, A., Winkler, W. C., Sondermann, H., and Lee, V. T. (2019) A dedicated diribonucleotidase resolves a key bottleneck for the terminal step of RNA degradation. *Elife* **8**, e46313
19. Vercruysse, M., Kohrer, C., Davies, B. W., Arnold, M. F., Mekalanos, J. J., RajBhandary, U. L., and Walker, G. C. (2014) The highly conserved bacterial RNase YbeY is essential in *Vibrio cholerae*, playing a critical role in virulence, stress regulation, and RNA processing. *PLoS Pathog.* **10**, e1004175
20. Ghosh, S., and Deutscher, M. P. (1999) Oligoribonuclease is an essential component of the mRNA decay pathway. *Proc. Natl. Acad. Sci. U. S. A.* **96**, 4372–4377
21. Srivastav, R., Sharma, R., Tandon, S., and Tandon, C. (2019) Role of DHH superfamily proteins in nucleic acids metabolism and stress tolerance in prokaryotes and eukaryotes. *Int. J. Biol. Macromol.* **127**, 66–75
22. Drexler, D. J., Muller, M., Rojas-Cordova, C. A., Bandera, A. M., and Witte, G. (2017) Structural and biophysical analysis of the soluble DHH/DHHA1-Type phosphodiesterase TM1595 from *Thermotoga maritima*. *Structure* **25**, 1887–1897.e4
23. Rao, F., See, R. Y., Zhang, D., Toh, D. C., Ji, Q., and Liang, Z. X. (2010) YybT is a signaling protein that contains a cyclic dinucleotide phosphodiesterase domain and a GGDEF domain with ATPase activity. *J. Biol. Chem.* **285**, 473–482
24. Mechold, U., Fang, G., Ngo, S., Ogryzko, V., and Danchin, A. (2007) YtqI from *Bacillus subtilis* has both oligoribonuclease and pAp-phosphatase activity. *Nucleic Acids Res.* **35**, 4552–4561
25. Wakamatsu, T., Kitamura, Y., Kotera, Y., Nakagawa, N., Kuramitsu, S., and Masui, R. (2010) Structure of RecJ exonuclease defines its specificity for single-stranded DNA. *J. Biol. Chem.* **285**, 9762–9769
26. Fisher, C. R., Wyckoff, E. E., Peng, E. D., and Payne, S. M. (2016) Identification and characterization of a putative manganese export protein in *Vibrio cholerae*. *J. Bacteriol.* **198**, 2810–2817
27. Srivastav, R., Kumar, D., Grover, A., Singh, A., Manjasetty, B. A., Sharma, R., and Taneja, B. (2014) Unique subunit packing in mycobacterial nanoRNase leads to alternate substrate recognitions in DHH phosphodiesterases. *Nucleic Acids Res.* **42**, 7894–7910
28. Uemura, Y., Nakagawa, N., Wakamatsu, T., Kim, K., Montelione, G. T., Hunt, J. F., Kuramitsu, S., and Masui, R. (2013) Crystal structure of the

ligand-binding form of nanoRNase from *Bacteroides fragilis*, a member of the DHH/DHHA1 phosphoesterase family of proteins. *FEBS Lett.* **587**, 2669–2674
29. He, Q., Wang, F., Liu, S., Zhu, D., Cong, H., Gao, F., Li, B., Wang, H., Lin, Z., Liao, J., and Gu, L. (2016) Structural and biochemical insight into the mechanism of Rv2837c from *Mycobacterium tuberculosis* as a c-di-NMP phosphodiesterase. *J. Biol. Chem.* **291**, 3668–3681
30. Koshland, D. E., Jr. (1959) Enzyme flexibility and enzyme action. *J. Cell. Comp. Physiol.* **54**, 245–258
31. Yang, J., Baek, M., and Seok, C. (2019) GalaxyDock3: Protein-ligand docking that considers the full ligand conformational flexibility. *J. Comput. Chem.* **40**, 2739–2748
32. Orr, M. W., Weiss, C. A., Severin, G. B., Turdiev, H., Kim, S. K., Turdiev, A., Liu, K., Tu, B. P., Waters, C. M., Winkler, W. C., and Lee, V. T. (2018) A subset of exoribonucleases serve as degradative enzymes for pGpG in c-di-GMP signaling. *J. Bacteriol.* **200**, e00300–e00318
33. Conner, J. G., Zamorano-Sanchez, D., Park, J. H., Sondermann, H., and Yildiz, F. H. (2017) The ins and outs of cyclic di-GMP signaling in *Vibrio cholerae*. *Curr. Opin. Microbiol.* **36**, 20–29
34. Tischler, A. D., and Camilli, A. (2004) Cyclic diguanylate (c-di-GMP) regulates *Vibrio cholerae* biofilm formation. *Mol. Microbiol.* **53**, 857–869
35. Heo, K., Park, Y. H., Lee, K. A., Kim, J., Ham, H. I., Kim, B. G., Lee, W. J., and Seok, Y. J. (2019) Sugar-mediated regulation of a c-di-GMP phosphodiesterase in *Vibrio cholerae*. *Nat. Commun.* **10**, 5358
36. Gao, J., Tao, J., Liang, W., Zhao, M., Du, X., Cui, S., Duan, H., Kan, B., Su, X., and Jiang, Z. (2015) Identification and characterization of phosphodiesterases that specifically degrade 3'3'-cyclic GMP-AMP. *Cell Res.* **25**, 539–550
37. Hallberg, Z. F., Wang, X. C., Wright, T. A., Nan, B., Ad, O., Yeo, J., and Hammond, M. C. (2016) Hybrid promiscuous (Hypr) GGDEF enzymes produce cyclic AMP-GMP (3', 3'-cGAMP). *Proc. Natl. Acad. Sci. U. S. A.* **113**, 1790–1795
38. Wright, T. A., Jiang, L., Park, J. J., Anderson, W. A., Chen, G., Hallberg, Z. F., Nan, B., and Hammond, M. C. (2020) Second messengers and divergent HD-GYP phosphodiesterases regulate 3',3'-cGAMP signaling. *Mol. Microbiol.* **113**, 222–236
39. Yadav, M., Pal, K., and Sen, U. (2019) Structures of c-di-GMP/cGAMP degrading phosphodiesterase VcEAL: Identification of a novel conformational switch and its implication. *Biochem. J.* **476**, 3333–3353
40. Kim, H. M., Park, Y. H., Yoon, C. K., and Seok, Y. J. (2015) Histidine phosphocarrier protein regulates pyruvate kinase A activity in response to glucose in *Vibrio vulnificus*. *Mol. Microbiol.* **96**, 293–305
41. Yoon, C. K., Kang, D., Kim, M. K., and Seok, Y. J. (2021) *Vibrio cholerae* FruR facilitates binding of RNA polymerase to the fru promoter in the presence of fructose 1-phosphate. *Nucleic Acids Res.* **49**, 1397–1410
42. Park, S., Park, Y. H., Lee, C. R., Kim, Y. R., and Seok, Y. J. (2016) Glucose induces delocalization of a flagellar biosynthesis protein from the flagellated pole. *Mol. Microbiol.* **101**, 795–808
43. Park, S., Yoon, J., Lee, C. R., Lee, J. Y., Kim, Y. R., Jang, K. S., Lee, K. H., and Seok, Y. J. (2019) Polar landmark protein HubP recruits flagella assembly protein FapA under glucose limitation in *Vibrio vulnificus*. *Mol. Microbiol.* **112**, 266–279
44. Choe, M., Min, H., Park, Y. H., Kim, Y. R., Woo, J. S., and Seok, Y. J. (2019) Structural insight into glucose repression of the mannitol operon. *Sci. Rep.* **9**, 13930
45. Choe, M., Park, Y. H., Lee, C. R., Kim, Y. R., and Seok, Y. J. (2017) The general PTS component HPr determines the preference for glucose over mannitol. *Sci. Rep.* **7**, 43431
46. Lee, J. W., Park, Y. H., and Seok, Y. J. (2018) Rsd balances (p)ppGpp level by stimulating the hydrolase activity of SpoT during carbon source downshift in *Escherichia coli*. *Proc. Natl. Acad. Sci. U. S. A.* **115**, E6845–E6854
47. Yongdae, J., Young-Ha, P., Jae-Woo, L., Inseong, J., Chaewoon, P., Yeong-Jae, S., and Nam-Chul, H. (2017) Purification, crystallization and preliminary X-ray crystallographic analysis of VCA0593 with a c-di-GMP binding activity in *Vibrio cholerae*. *Biodesign* **5**, 70–73
48. Otwinowski, Z., and Minor, W. (1997) Processing of X-ray diffraction data collected in oscillation mode. *Methods Enzymol.* **276**, 307–326
49. Adams, P. D., Afonine, P. V., Bunkoczi, G., Chen, V. B., Davis, I. W., Echols, N., Headd, J. J., Hung, L. W., Kapral, G. J., Grosse-Kunstleve, R. W., McCoy, A. J., Moriarty, N. W., Oeffner, R., Read, R. J., Richardson, D. C., *et al.* (2010) Phenix: A comprehensive python-based system for macromolecular structure solution. *Acta Crystallogr. D Biol. Crystallogr.* **66**, 213–221
50. Emsley, P., and Cowtan, K. (2004) Coot: Model-building tools for molecular graphics. *Acta Crystallogr. D Biol. Crystallogr.* **60**, 2126–2132
51. Park, H., Lee, G. R., Heo, L., and Seok, C. (2014) Protein loop modeling using a new hybrid energy function and its application to modeling in inaccurate structural environments. *PLoS One* **9**, e113811
52. Miller, V. L., and Mekalanos, J. J. (1988) A novel suicide vector and its use in construction of insertion mutations: Osmoregulation of outer membrane proteins and virulence determinants in *Vibrio cholerae* requires *toxR*. *J. Bacteriol.* **170**, 2575–2583
53. Milton, D. L., O'Toole, R., Horstedt, P., and Wolf-Watz, H. (1996) Flagellin A is essential for the virulence of *Vibrio anguillarum*. *J. Bacteriol.* **178**, 1310–1319
54. Lim, J. G., Bang, Y., and Choi, S. H. (2014) Characterization of the *Vibrio vulnificus* 1-Cys peroxiredoxin Prx3 and regulation of its expression by the Fe-S cluster regulator IscR in response to oxidative stress and iron starvation. *J. Biol. Chem.* **289**, 36263–36274